# Effect of the Effective Metal Surface Area of Two Different Flow Diverter Stents on the Stagnation Region Formation Inside the Aneurysm Sac

Muhammed Talha Gunaydin[1]    Gorkem Guclu[1]    Ali Bahadir Olcay[1]    Atakan Orscelik[2]    Cem Bilgin[3]
Bahattin Hakyemez[4]

[1] Department of Mechanical Engineering, Faculty of Engineering, Yeditepe University, Istanbul, Türkiye
[2] Department of Neurological Surgery, University of California, San Francisco, San Francisco, California, United States
[3] Department of Radiology, Mayo Clinic, Rochester, Minnesota, United States
[4] Department of Radiology, Uludag University School of Medicine, Bursa, Türkiye

**Address for correspondence** Atakan Orscelik, MD, Department of Neurological Surgery, University of California, San Francisco, 400 Parnassus Avenue, 8th Floor, San Francisco, CA 94143, United States (e-mail: atakanorscelik@gmail.com).

## Abstract

**Objective**    Flow diversion (FD) is a relatively new technique for treating large, wide-necked, or fusiform aneurysms. Although FD is a more preferred option than coiling or clipping techniques in neurosurgery and neuroradiology clinics, the blood flow mechanism inside the aneurysm sac is not fully understood after the treatment. Besides, effective metal surface area (EMSA), a property of an FD related to porosity, shows variation at the patient's aneurysm neck by providing more or less blood flow inside an aneurysm sac than planned, causing nonstagnant or stagnant fluid region formation in the sac, respectively. Thus, the change in FD's EMSA can significantly affect the treatment's effectiveness, making even operation unsuccessful when variation in FD's EMSA at the aneurysm neck is overlooked.

**Materials and Methods**    In this study, a large aneurysm of a 52-year-old female patient was numerically investigated by virtually placing two commercially available FDs with different EMSA values one by one into the aneurysm-carrying artery.

**Results**    While FD stents at the aneurysm site substantially reduced the blood flow into the aneurysm, an FD with a 15.6% EMSA caused blood to flow in the aneurysm sac to have six times more kinetic energy than that of FD with a 29.5% EMSA.

**Conclusion**    Although FD's EMSA value demonstrated nearly up to 20% reduction at the patient's aneurysm neck based on a product catalog value, numerical model results revealed that the stagnated region's formation inside the aneurysm sac could be determined within a 9% difference based on digital subtraction angiography reformat image.

### Keywords
► effective metal surface area
► internal carotid artery aneurysm
► flow diverter stent
► patient-specific
► CFD modeling

## Introduction

Flow diverter (FD) reduces the blood flow within the aneurysm sac and, thus, leads to aneurysmal occlusion. Therefore, FD is frequently used for giant, wide-necked, or fusiform aneurysms, challenging to treat with coiling.[1–4] Different prospective studies have demonstrated the FD's safety and efficacy.[5–11] Hence, FD has become one of the newest techniques in endovascular aneurysm treatment. However, the mechanisms of complications are poorly understood, and even in an asymptomatic patient, fatal complications can occur due to FD in the clinics. Therefore, further investigations are needed to clarify the hemodynamic effects of FD.

The effective metal surface area (EMSA) value of the FD and the geometry and aspect ratio of the aneurysm generally determine changes in intra-aneurysmal blood flow.[8,12,13] EMSA values of the same-sized FDs may differ depending on the parent artery's anatomy and the FD's wire configuration.[8,12–15] If the value of EMSA is too low, the FD will not significantly decrease intra-aneurysmal blood flow. On the other hand, overly increased EMSA will further prevent blood from flowing into the sac and may cause focal low wall shear stress (WSS) areas and an aneurysm rupture[16,17]; hence, EMSA values can directly affect the treatment outcome. These results suggest that in contrast to the pathogenic effect of a high WSS in the initiating phase, a low WSS may facilitate the growing phase and trigger the rupture of a cerebral aneurysm by causing degenerative changes in the aneurysm wall. The WSS of the aneurysm region may be of some help for the prediction of rupture.[16] In addition, FD's pore density values are proportionally affected by the EMSA values. This means that the pore density effects would be the same as those of the EMSA values.

In this study, the postdeployment changes in the EMSA values were calculated for asymptomatic, large supraclinoid aneurysms. Besides, the intra-aneurysmal blood flow with these EMSA values was investigated to understand the effect of EMSA on blood flow behavior in the aneurysm sac. Prediction of the EMSA values that will occur after deployment of the FD may select the most effective FD yielding a patient-specific solution. Furthermore, these values can be used to predict treatment outcomes. The additional benefit of this method is that patients who will not benefit from FD can be identified, and unnecessary periprocedural complications can be prevented for those patients.

## Materials and Methods

A 52-year-old female patient with a worsened headache in the last 3 months was guided to the clinic. Although the clinical neurological evaluation was routine, magnetic resonance imaging showed an aneurysm in her supraclinoid segment of the right internal carotid artery, as shown in ►Fig. 1A and B. It was decided to continue with a FD of FRED4017[18] because of the size and wide-necked nature of the aneurysm. After the FD placement, immediate stagnation was observed in digital subtraction angiography (DSA) images. It was noticed that patient's symptoms disappeared, and the control angiography revealed total aneurysmal occlusion in the third-month follow-up. Lastly, no recanalization was observed at the sixth-month follow-up angiography.

The aneurysm shown in ►Fig. 1B was virtually cut into three identical volumes, as seen in ►Fig. 1C. Therefore, fluid flow properties such as velocity vector fields and dynamic viscosity contour plots at the aneurysm sac's top, middle, and bottom sections can be monitored in more detail.[19] Once the three-dimensional geometry was obtained from Digital Imaging and Communications in Medicine images, the virtual stent deployment method was performed by placing 64 wire-braid (i.e., 48 inner and 16 outer wires) FRED4017[18] and 48 wire-braid Product A[20] FD stents to the aneurysm neck, one by one as given in ►Fig. 1D, while the details of virtual stent deployment method into a patient-specific data were discussed in some other studies.[21–23] The diameters of the inner and outer wires of FRED4017 are 22.5 and 56 µm, respectively. On the other hand, Product A FD stent wires are identical to each other, and their diameter is 25 µm. The patient's average artery diameter where the aneurysm was located was measured to be 3.5 mm. EMSA values of FRED4017 and Product A FD stents are obtained to be 32 and 18.8%, respectively, when they are placed in a 3.5-mm parent artery.[18,20] Although these EMSA values are described in product catalogs, it was discovered that EMSA value could change drastically at the aneurysm's neck due to the parent artery's curly and nonuniform shape.[19] Therefore, when FRED4017 is placed into the patient's aneurysm site, the stent's EMSA value decreases from 32 to 29.5% at the aneurysm neck. Similarly, the EMSA value of Product A drops from 18.8 to 15.6% at the aneurysm neck when this stent is positioned at the patient's aneurysm site.

In the numerical model, the working fluid was chosen as blood with a density of 1047 kg/m$^3$ and a molar mass of 64.458 g/mol. Blood was introduced as a non-Newtonian Bird-Carreau model with high and low shear viscosity values of 0.0035 and 0.056 Pa.s, respectively.[24–26] The usage of antithrombotic drugs and their effects are neglected.[27] The flow was assumed to be laminar since the highest Reynolds number in the artery was only 321. An in-house MATLAB code was generated to employ the Womersley velocity profile to the inlet of the computational domain,[28,29] while the artery outlets were defined as openings, as seen in ►Fig. 1C with an 80 mm Hg pressure. The walls of the parent artery and aneurysm were defined as a rigid wall. An *XZ* plane was created, as illustrated in ►Fig. 1E, to provide a comparison between DSA images with computational fluid dynamics (CFD) simulation results.

Mesh independency tests were also performed for a half cardiac cycle (0.4 seconds) long with 22, 27, and 35 M elements. In these tests, the 27 M element numerical model's mesh size shown in ►Fig. 1F was chosen since the difference in mean dynamic viscosities was less than
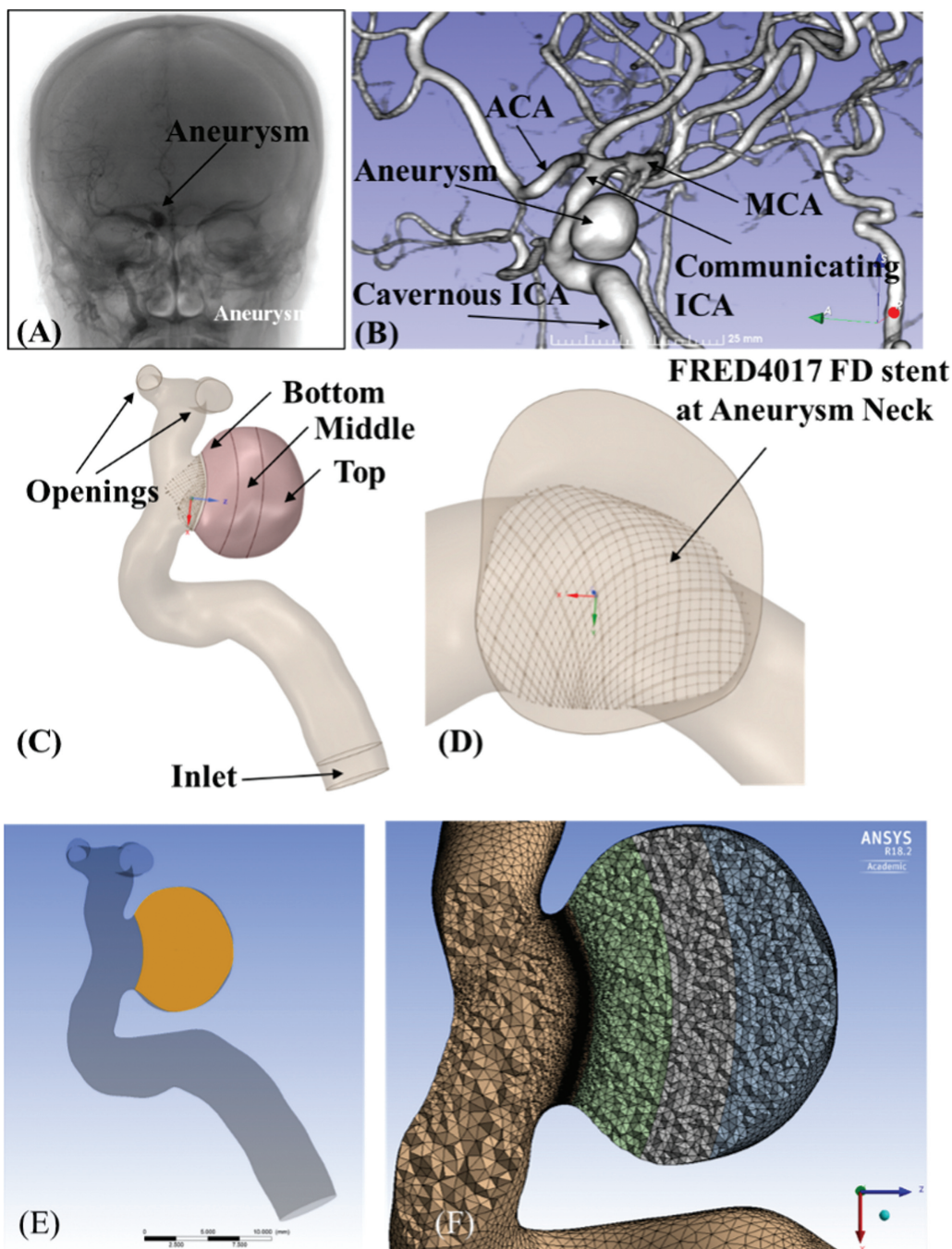
**Fig. 1** A 52-year-old female patient's front skull view with aneurysm (**A**). Three-dimensional (3D) rendered view of patient's parent arteries, (**B**). 3D computational fluid dynamics (CFD) domain having one inlet and two outlets with three regions of the aneurysm (**C**). Enlarged view of aneurysm neck and FRED4017 flow diverter (FD) stent's wire mesh structure (**D**). Plane *XZ* was formed to provide a comparison between digital subtraction angiography (DSA) images and CFD simulation results (**E**). Cross-section mesh view of the aneurysm site where FRED4017 FD stent was virtually deployed (**F**).

5% compared with the 35 M elements model. It is noted that the average skewness was 0.23, while the average orthogonal quality was 0.77. A time convergence test was also performed, and the time step size of 0.005 seconds was determined to be used since the blood flow in the artery was defined as a time-dependent velocity profile. The total simulation time was five cardiac cycles long, yielding 4 seconds after stent placement into the patient's aneurysm site.

## Results and Discussion

DSA images of the patient before FD deployment are presented in the first column of ►**Fig. 2**, while tangential velocity vectors and dynamic viscosity plots are provided in the second and third columns of ►**Fig. 2**, respectively, for 0, 0.2, 0.4, and 0.8 seconds of the 5th cardiac cycle of the simulation. It is seen from the first and second columns of ►**Fig. 2** that blood flow first enters and fills inside the
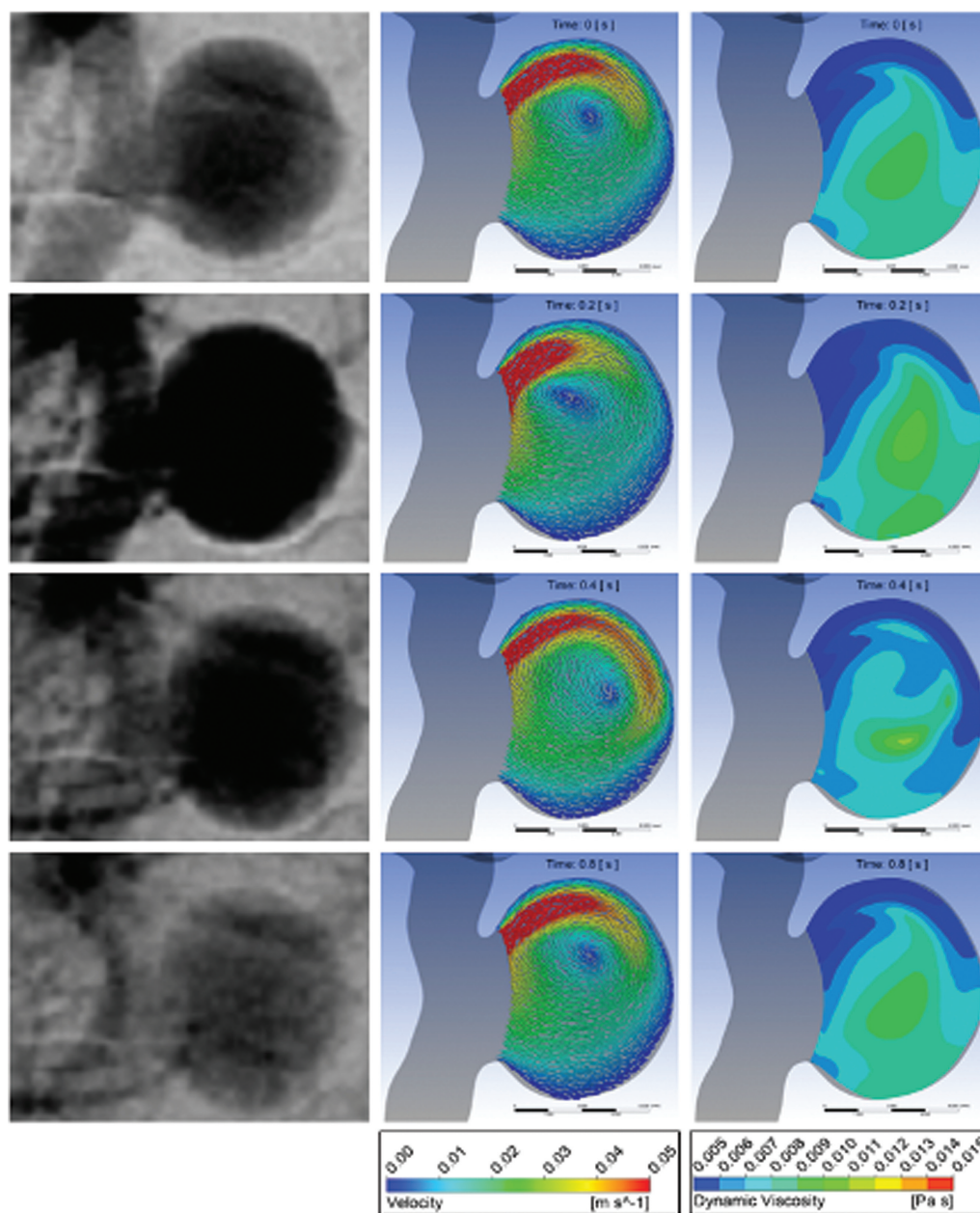
**Fig. 2** Digital subtraction angiography (DSA) images before a flow diverter (FD) stent deployment (**A**). Tangential velocity vectors (**B**). Dynamic viscosity contours (**C**) at plane *XZ* for 0, 0.2, 0.4, and 0.8 seconds of the 5th cycle of the simulation. Time values given at the top of computational fluid dynamics (CFD) images indicate the time evolution of tangential velocity vectors and dynamic viscosity at the *XZ* plane of the aneurysm sac.

aneurysm; then, it leaves the aneurysm sac since incoming flow pushes the blood already in the aneurysm. Dynamic viscosity plots in ►**Fig. 2** indicate that viscosity decreases in places where blood flow is fast, implying that no stagnation can be obtained at those high shear rate places.

FD stents are designed so that once they are placed into an aneurysm site, most of the incoming flow is diverted into the main vessel, and only a small portion of the blood is allowed to enter inside the aneurysm. In this part of the study, mean velocity (►**Fig. 3A**), viscosity (►**Fig. 3B**), WSS (►**Fig. 3C**), and kinetic energy (►**Fig. 3D**) values are obtained to quantify the effect of FD use inside the aneurysm for before and after

surgery at the top, middle, and bottom of the aneurysm sac. First, the FD stent use drastically reduces the blood flow into the aneurysm, as expected for both Product A and FRED4017. Second, when the effect of these two FD stents is compared, FRED4017 provides more FD into the main vessel compared with that of Product A because FRED4017 has a higher EMSA value than Product A. Use of FD stent also decreases flow velocity inside an aneurysm by initiating a stagnation region formation. Besides, when the shear rate declines inside the aneurysm sac, blood viscosity increases due to the shear-thinning behavior of blood. ►**Fig. 3B** indicates that viscosity in FRED4017 use is nearly 50% more than that of Product A.
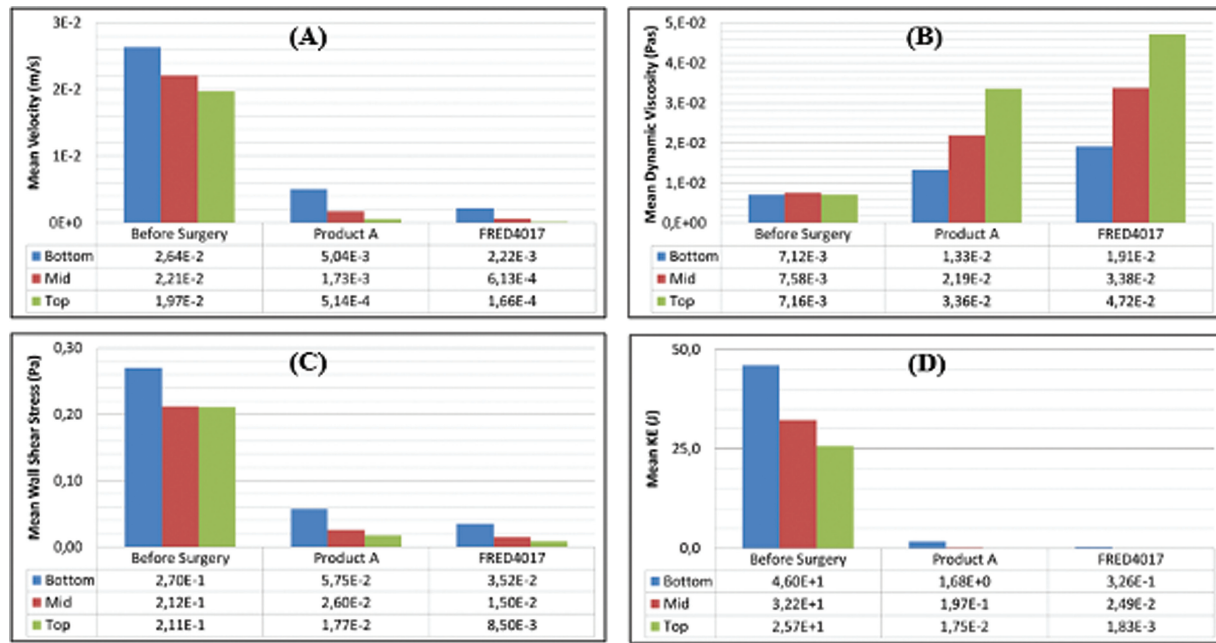
**Fig. 3** Computational fluid dynamics (CFD) results for mean velocity (**A**), mean dynamic viscosity (**B**), mean wall shear stress (WSS) (**C**), and kinetic energy (**D**) for no-stent, virtually deployed Product A, and FRED4017 flow diverter (FD) stent cases in aneurysm sac regions (bottom, mid, top). Note that all CFD simulations in ►**Fig. 3** were taken inside the volume of the aneurysm sac at the 5th cardiac cycle.

Furthermore, the maximal hydraulic resistance occurs where the fibrinogen concentration is high.[30] Since hydraulic resistance and dynamic viscosity are related to each other, high-viscosity areas have a higher chance of starting the blood clotting process. When an FD stent is implanted into an aneurysm's neck, WSS at the aneurysm wall is directly decreased by reducing the bleeding or rupture risks. Therefore, both Product A and FRED4017 exhibit excellent performance in reducing WSS values inside the aneurysm sac, as shown in ►**Fig. 3C**.

Lastly, the mean kinetic energy inside the aneurysm sac is calculated using $K.E = \frac{1}{2}\rho V v^2$. Here, $K.E$ is the kinetic energy, $\rho$ is the density of blood, $V$ is the volume of the interested region, and $v$ is the mean velocity. ►**Fig. 3D** illustrates the kinetic energy values inside the aneurysm sac before and after the FD stent placement. Specifically, mean kinetic energy inside the aneurysm sac was found to be 34.63, 0.631, and 0.118 J, respectively, for no-stent, virtually deployed Product A, and FRED4017 FD cases. This implies that if Product A was placed into the patient's aneurysm neck, blood flow would have nearly six times more kinetic energy compared with that of FRED4017. Hence, the loss of the kinetic energy inside the aneurysm sac can be directly associated with stagnation region formation and, eventually, blood coagulation initiation.

The first column of ►**Fig. 4** shows DSA images taken just after FRED4017 FD deployment in the clinic. While gray regions inside the aneurysm sac marked as a nonstagnated region indicate blood flow entering the sac, the black area inside the sac shows a stagnated blood region. Therefore, it can be seen that although blood flow enters inside the aneurysm sac, it can hardly move on to the top part of the

aneurysm because there is already stagnated blood formed at the top aneurysm region, as illustrated in ►**Fig. 4A**. Since a portion of blood enters the sac, the same amount must leave the sac to satisfy the conservation of mass principle. However, blood at the middle and top region of the aneurysm sac cannot escape since blood at these locations has minimal kinetic energy.

Velocity vector plots obtained from CFD simulations are given in ►**Fig. 4B**. It is noted that the blood velocity after FD stent placement is minimal compared with blood velocity for the no-stent case. Furthermore, DSA images obtained after FD stent placement (►**Fig. 4A**) agree well with velocity vector plots (►**Fig. 4B**) in the identification of nonstagnated and stagnated fluid regions. On the other hand, blood's dynamic viscosity shows large values (►**Fig. 4C**) in a place where blood velocity is low.

In neurosurgery and neuroradiology clinics, the doctors can plan to have a stagnation region inside the aneurysm sac once s/he places an FD stent into the aneurysm site of a patient because stagnation region formation is generally associated with blood clotting initiation and healing time of aneurysm. ►**Fig. 5A** shows a DSA reformat image of the aneurysm sac taken after FRED4017 FD stent placement, while ►**Fig. 5B** illustrates a high dynamic viscosity region at 0.1 seconds of the simulation's 5th cardiac cycle. The stagnation region's volume is 265 and 242.2 mm³ from the DSA reformat image and dynamic viscosity contour plot, respectively. It is noted that the difference between these two volume calculations is less than 9%. Thus, CFD simulations can provide promising blood flow behavior results in the aneurysm sac for the interventional radiologist before an FD stent placement.
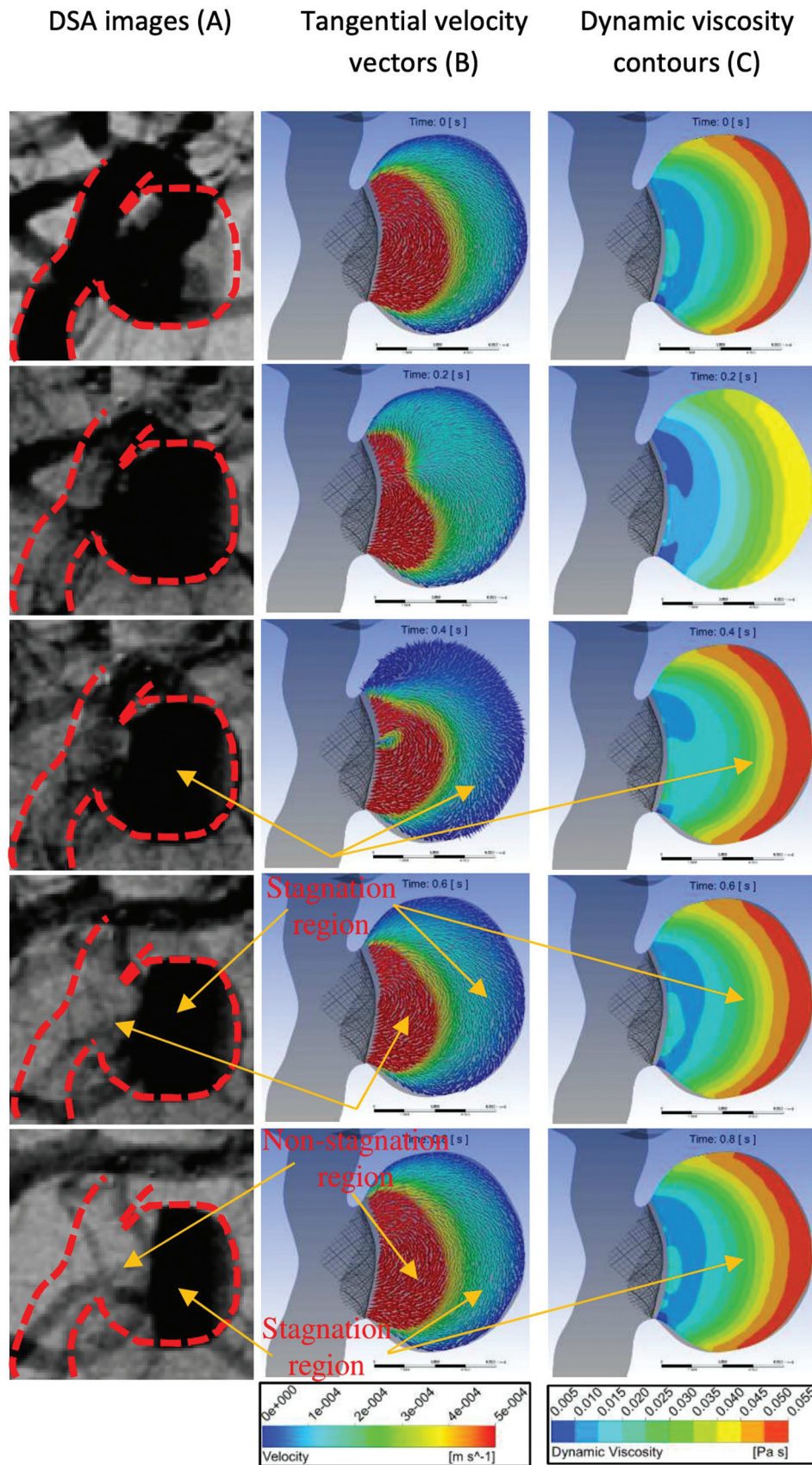
**Fig. 4** Digital subtraction angiography (DSA) images just after FRED4017 flow diverter (FD) stent deployment in the clinic (**A**). Tangential velocity vectors (**B**). Dynamic viscosity contours (**C**). Note that all computational fluid dynamics (CFD) simulations in ►**Fig. 4** were run after a virtual FRED4017 FD stent deployment case, shown at plane *XZ*, and taken at 0, 0.2, 0.4, 0.6, and 0.8 seconds of the 5th cycle of the simulation. Time values given at the top of CFD images indicate the time evolution of tangential velocity vectors and dynamic viscosity at the *XZ* plane of the aneurysm sac.
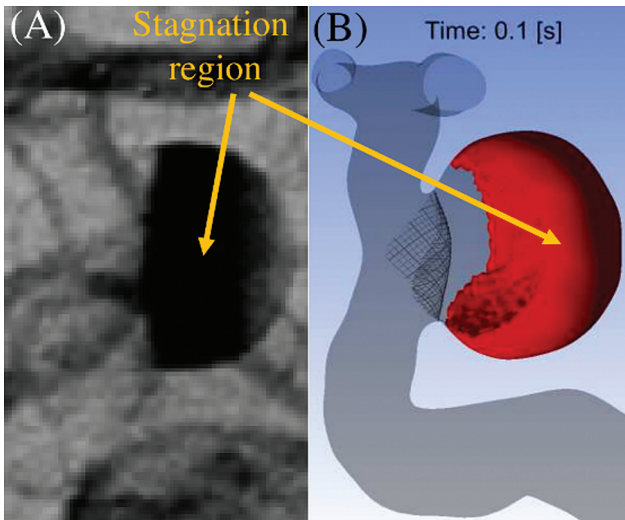
**Fig. 5** The stagnation region formation after FRED4017 placement into the aneurysm site: digital subtraction angiography (DSA) reformat image showing stagnation of contrast fluid (**A**). Blood with high viscosity region in the aneurysm sac (**B**).

## Conclusion

In this study, a large aneurysm of a 52-year-old female patient was numerically investigated by placing two commercially available FD stents with different EMSA values into the aneurysm site. While the FRED4017 FD stent was deployed into the patient's aneurysm neck in the clinic, both Product A and FRED4017 were virtually knitted inside the patient's aneurysm-carrying parent artery one by one. It was realized that the EMSA value of FRED4017 declined from 32 to 29.5% at the aneurysm neck, yielding more blood flow into the sac than intended. Numerical results also show that Product A's EMSA value dropped from 18.8 to 15.6% at the aneurysm neck, allowing more massive blood flow into the aneurysm sac than that of FRED4017.

On the other hand, mean velocity and dynamic viscosity in the aneurysm sac before and after FD stent placements were obtained from numerical models to quantify the effect of EMSA on the stagnation region formation in the aneurysm sac. Therefore, blood viscosity values in the sac of the FRED4017 case were calculated to be nearly 50% more than that of Product A, indicating an initial phase of the blood clotting process since the formation and evaluation of the stagnation region in the sac are generally associated with dynamic viscosity.[19,26,31,32] Thus, a large stagnation region was obtained in the patient's aneurysm sac when the FRED4017 FD stent was employed instead of Product A.

Although the FRED4017 FD stent was placed into the patient's aneurysm neck in the clinic, WSS, an indicator of the aneurysm bleeding or rupture risk, was evaluated to be low for both FD stents. Lastly, the volume comparison of the stagnated zone of the DSA reformat image and high viscous region of fluid flow gave less than a 9% difference, implying that the shear thinning behavior of blood can be used to identify stagnated fluid flow zones in the aneurysm sac.

## References

1 Chalouhi N, Tjoumakaris S, Starke RM, et al. Comparison of flow diversion and coiling in large unruptured intracranial saccular aneurysms. Stroke 2013;44(08):2150–2154

2 Zanaty M, Chalouhi N, Starke RM, et al. Flow diversion versus conventional treatment for carotid cavernous aneurysms. Stroke 2014;45(09):2656–2661

3 Simgen A, Roth C, Kulikovski J, et al. Endovascular treatment of unruptured intracranial aneurysms with flow diverters: a retrospective long-term single center analysis. Neuroradiol J 2023;36 (01):76–85

4 Piano M, Lozupone E, Milonia L, et al. Flow diverter devices in the treatment of complex middle cerebral artery aneurysms when surgical and endovascular treatments are challenging. J Stroke Cerebrovasc Dis 2022;31(12):106760

5 Meyers PM, Coon AL, Kan PT, Wakhloo AK, Hanel RA. SCENT trial. Stroke 2019;50(06):1473–1479

6 Hanel RA, Kallmes DF, Lopes DK, et al. Prospective study on embolization of intracranial aneurysms with the pipeline device: the PREMIER study 1 year results. J Neurointerv Surg 2020;12 (01):62–66

7 Pierot L, Spelle L, Berge J, et al. SAFE study (Safety and efficacy Analysis of FRED Embolic device in aneurysm treatment): 1-year clinical and anatomical results. J Neurointerv Surg 2019;11(02): 184–189

8 Altındağ B, Bahadır Olcay A, Furkan Tercanlı M, Bilgin C, Hakyemez B. Determining flow stasis zones in the intracranial aneurysms and the relation between these zones and aneurysms' aspect ratios after flow diversions. Interv Neuroradiol 2023; 159101992311628:15910199231162878

9 Lobotesis K, Downer J, Chandran A, et al. FRED-UK: Safety and efficacy analysis of FRED™/FRED™ Jr embolic device in aneurysm

treatment – efficacy and safety results at 12–24 months. J Neurointerv Surg 2022;14:A2–A3

10 Hanel RA, Cortez GM, Lopes DK, et al. Prospective study on embolization of intracranial aneurysms with the pipeline device (PREMIER study): 3-year results with the application of a flow diverter specific occlusion classification. J Neurointerv Surg 2023; 15:248–254

11 Soydemir E, Gündoğmuş CA, Türeli D, Andaç Baltacıoğlu N, Bayri Y, Baltacıoğlu F. Safety and efficacy of flow diverter stents in the treatment of middle cerebral artery aneurysms: a single-center experience and follow-up data. Diagn Interv Radiol 2023;29(02): 350–358

12 Wang K, Yuan S. Actual metal coverage at the neck is critical for flow-diverting stents in treating intracranial aneurysms. AJNR Am J Neuroradiol 2013;34(03):E31–E32

13 Wang K, Huang Q, Hong B, Li Z, Fang X, Liu J. Correlation of aneurysm occlusion with actual metal coverage at neck after implantation of flow-diverting stent in rabbit models. Neuroradiology 2012;54(06):607–613

14 Shapiro M, Raz E, Becske T, Nelson PK. Variable porosity of the pipeline embolization device in straight and curved vessels: a guide for optimal deployment strategy. AJNR Am J Neuroradiol 2014;35(04):727–733

15 Zhang X, Hao W, Han S, et al. Middle cerebral arterial bifurcation aneurysms are associated with bifurcation angle and high tortuosity. J Neuroradiol 2022;49(05):392–397

16 Shojima M, Oshima M, Takagi K, et al. Magnitude and role of wall shear stress on cerebral aneurysm:computational fluid dynamic study of 20 middle cerebral artery aneurysms. Stroke 2004;35 (11):2500–2505

17 Zhou G, Zhu Y, Yin Y, Su M, Li M. Association of wall shear stress with intracranial aneurysm rupture: systematic review and meta-analysis. Sci Rep 2017;7(01):5331

18 Microvention Terumo Fred Product Catalog. Flow Re-Direction Endoluminal Device Flow Re-Direction Endoluminal Device FRED ® System Effective Metal Surface Area. Tustin, CA 92780, USA: 2015

19 Ünsal C, Güçlü G, Olcay AB, Hassankhani A, Bilgin C, Hakyemez B. How flow diverter selection can affect the flow changes within a jailed ophthalmic artery: a computational fluid dynamics study. Asian J Neurosurg 2024;19(03):426–434

20 Surpass Flow Diverter Selection Guide. Copyright © Stryker 90816304.AE, 2nd Page, Mesh Density Comparison Plot; 2013

21 Damiano RJ, Tutino VM, Paliwal N, et al. Compacting a single flow diverter versus overlapping flow diverters for intracranial aneur-

ysms: a computational study. AJNR Am J Neuroradiol 2017;38 (03):603–610

22 Janiga G, Daróczy L, Berg P, Thévenin D, Skalej M, Beuing O. An automatic CFD-based flow diverter optimization principle for patient-specific intracranial aneurysms. J Biomech 2015;48 (14):3846–3852

23 Nishimura K, Otani K, Mohamed A, et al. Accuracy of length of virtual stents in treatment of intracranial wide-necked aneurysms. Cardiovasc Intervent Radiol 2019;42(08):1168–1174

24 Jahangiri M, Saghafian M, Sadeghi MR. Effects of non-Newtonian behavior of blood on wall shear stress in an elastic vessel with simple and consecutive stenosis. Biomed Pharmacol J 2015; 8:123–131

25 Hippelheuser JE, Lauric A, Cohen AD, Malek AM. Realistic non-Newtonian viscosity modelling highlights hemodynamic differences between intracranial aneurysms with and without surface blebs. J Biomech 2014;47(15):3695–3703

26 Mutlu O, Olcay AB, Bilgin C, Hakyemez B. Evaluating the effects of the wire number of flow diverter stents on the non-stagnated region formation in an aneurysm sac using Lagrangian coherent structure and hyperbolic time analysis. World Neurosurg 2020; 133:e666–e682

27 Tercanlı MF, Olcay AB, Mutlu O, Bilgin C, Hakyemez B. Investigation of the effect of anticoagulant usage in the flow diverter stent treatment of the patient-specific cerebral aneurysm using the Lagrangian coherent structures. J Clin Neurosci 2021; 94:86–93

28 Womersley JR. Method for the calculation of velocity, rate of flow and viscous drag in arteries when the pressure gradient is known. J Physiol 1955;127(03):553–563

29 Pashaei A, Fatouraee N. An analytical phantom for the evaluation of medical flow imaging algorithms. Phys Med Biol 2009;54(06): 1791–1821

30 Govindarajan V, Rakesh V, Reifman J, Mitrophanov AY. Computational study of thrombus formation and clotting factor effects under venous flow conditions. Biophys J 2016;110(08):1869–1885

31 Mutlu O, Olcay AB, Bilgin C, Hakyemez B. Evaluating the effectiveness of 2 different flow diverter stents based on the stagnation region formation in an aneurysm sac using Lagrangian coherent structure. World Neurosurg 2019;127:e727–e737

32 Mutlu O, Olcay AB, Bilgin C, Hakyemez B. Understanding the effect of effective metal surface area of flow diverter stent's on the patient-specific intracranial aneurysm numerical model using Lagrangian coherent structures. J Clin Neurosci 2020; 80:298–309